Improvement in threshold of In Ga N Ga N quantum-well lasers by p -type modulation doping

Shyh-Jer Huang and Shun-Tung Yen

Citation: Journal of Applied Physics **102**, 113103 (2007); doi: 10.1063/1.2818366
View online: http://dx.doi.org/10.1063/1.2818366
View Table of Contents: http://scitation.aip.org/content/aip/journal/jap/102/11?ver=pdfcov
Published by the AIP Publishing

Improvement in threshold of InGaN/GaN quantum-well lasers by *p*-type modulation doping

Shyh-Jer Huang and Shun-Tung Yen[a)]
Department of Electronics Engineering, National Chiao Tung University, Hsinchu, Taiwan 30050, Republic of China

(Received 16 July 2007; accepted 5 October 2007; published online 4 December 2007)

The optical properties of modulation-doped InGaN/GaN laser diodes are theoretically studied with the effects of electron spillover from quantum wells considered. We use a six-band model including the strain effect for calculating valence band states. The continuous subbands are treated by a dense discretization for the electrons spilling from the quantum wells. The calculation results show that the threshold current can be significantly reduced by *p*-type modulation doping around the wells but not by *n*-type doping, supposed that the layers are of a perfect quality and the impurity-induced defects are ignored. Also, the *p*-type modulation doping can make the threshold current more insensitive to the cavity loss compared with other cases. An optimized threshold current density can be achieved for single-quantum-well lasers by introducing *p*-type dopants. However, the dopant concentration is high and may be inaccessible. For double-quantum-well lasers an optimized low threshold current can be achieved with a slighter and practicable *p*-type doping level. © *2007 American Institute of Physics*. [DOI: 10.1063/1.2818366]

I. INTRODUCTION

In the last decades, the material preparation and device processing technologies in the nitride-based blue light source have made great progress.[1–3] The short-wavelength light-emitting diodes and laser diodes (LDs) have recently been made up commercially by GaN and the related ternary (AlGaN and InGaN) and quaternary (AlGaInN) compounds due to their potential applications in full-color displays and high-density optical storage. However, the reliability is still a critical issue for the wide-gap nitride LDs because of the short lifetime resulting from the high threshold current. In order to reduce the threshold current, further improvements in material preparation and device processing technologies are still required to eliminate the undesired defects in the active region. In addition, the optimization on the LD structure is also required to diminish the leakage current resulting from the spillover of carriers, including the electron leakage from the active region to the *p*-type cladding layer, and the loss of high-energy electrons due to interband recombinations. The high-energy electrons generally occupy the continuous subband states and therefore give only a small contribution to the optical peak gain.

It has been found in recent works that inserting an AlGaN electron blocking layer (EBL) between the active region and the *p*-type cladding layer can reduce the electron leakage from the active region.[4–7] Besides, more efforts can be made for further reducing the threshold current. For example, one can introduce dopants into the active region. Actually, *n*-type doping with Si in the InGaN/GaN quantum wells (QWs) has been performed in some experimental works.[8–10] It is found that the Si doping can improve the crystalline quality of GaN layers and the InGaN/GaN interface.[11] It is well known that the optimized temperature for the high crystalline quality of InGaN wells is lower than that suitable for the growth of GaN barriers. In order to get high quality of InGaN wells the GaN layers are generally compelled to be grown at low temperature. Hence, this forms the islandlike spiral defects initiated by threading dislocations existing in the underlying GaN template. Fortunately, workers found that introducing Si impurities can dramatically suppress these islandlike spiral structures of GaN layers. However, the *n*-type doping causes a large amount of electrons occupying high-energy states at threshold and leads to serious spillover of electrons. A high barrier of EBL is then needed to prevent the energetic electrons from leaking into the *p*-type cladding layer, but this gives rise to a reduction in optical confinement within the active region. From this point of view, the *p*-type doping should be a better choice than the *n*-type doping because it can reduce the number of spillover electrons at threshold. However, there are few experimental or theoretical works concerning the optical property of the *p*-type doped active region in InGaN/GaN QW LDs. In order to further improve the performance of the InGaN/GaN QW LDs, it is worthwhile to investigate the influence of *p*-type doping on the optical property of the active region.

In this paper, we investigate theoretically in detail the influence of different species (the *n* type and *p* type) and various levels of doping to the active region on the spontaneous emission rate and the threshold current density of InGaN/GaN LDs. Our results demonstrate that the amount of spillover electrons at threshold can indeed strongly depend on the species and the level of doping. Accordingly, we can obtain a low threshold current by optimizing the doping level with a preferred doping species. The paper is organized as follows. The calculation method is described briefly in the next section. Then, the results and discussions follow. Finally, the conclusion is drawn.

[a)]Electronic mail: styen@mail.nctu.edu.tw

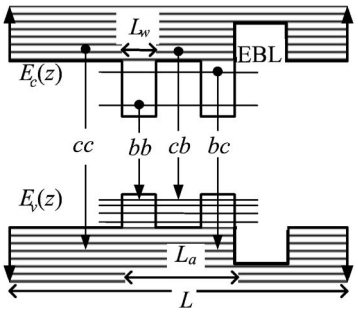

FIG. 1. Schematic illustration of the band diagram of the neighborhood of the InGaN/GaN QW active region inside which four different kinds (bb, cb, bc, and cc) of interband processes occur. The cb (bb) process means the interband process between the continuous (bound) conduction and the bound valence subbands, while the bc (cc) means the process between the bound (continuous) conduction and the continuous valence subbands. The well has a width L_w and the active region has a width L_a. The continuous subbands are simulated by dense discrete subbands that are discretized using two infinite potential boundaries. An AlGaN EBL is put immediately near the active region.

II. CALCULATION APPROACHES

We consider lasers with a conventional separate confinement heterostructure containing an active region of strained InGaN/GaN QWs, as illustrated in Fig. 1. An AlGaN EBL is inserted immediately near the QWs. The layers are assumed to be grown on strain-free GaN substrate along the crystallographic c axis which is defined as the z axis. The strain-induced piezoelectric field may be important in InGaN/GaN QWs. However, because the threshold carrier density in the InGaN/GaN QWs is generally large (in the range of $10^{19}-10^{20}$ cm^{-3}), the piezoelectric field is strongly suppressed by the carrier screening at threshold. It has been pointed out that in the range of so high carrier densities the transition energy between the lowest conduction and valence subbands changes slightly with the carrier density.[12] Its value approximates to that in the fully screening case. The almost fully screening of the polarization-induced electric field was also demonstrated experimentally in nitride LDs close to the threshold condition.[13] So, the flatband profile is assumed in calculation for convenience.

The calculation approaches mainly follow those given in our previous work,[14] except that we consider modulation doping to the active region in this study. For convenience, we give a brief description of the calculation approaches here. We consider two types of subbands here as similar to those in Ref. 15. They are the bound subbands confined to the well and the continuous subbands (unconfined to the well) with the edges higher than the barrier in energy. The way to deal theoretically with the continuous subbands has been described in detail elsewhere.[15,16] In the practical calculation, we impose fictitious infinite potential barriers far away from the active region to make the discrete subbands above the barrier dense enough to resemble the continuous subbands. Hence, the interband optical transitions can be categorized into four parts: (1) the bound to bound (bb), (2) the bound to continuous (bc), (3) the continuous to bound (cb), and (4) the continuous to continuous (cc) transitions, as indicated in Fig. 1. The gain g, the spontaneous emission rate r_{sp}, and the current density J therefore can also be regarded as composed of four components associated with the four kinds of optical transitions mentioned above; that is, $g=g_{bb}+g_{cb}+g_{bc}+g_{cc}$, $r_{sp}=r_{sp,bb}+r_{sp,cb}+r_{sp,bc}+r_{sp,cc}$, and $J=J_{bb}+J_{cb}+J_{bc}+J_{cc}$, where the subscripts indicate the kinds of optical transitions.

In most theoretical studies of QW lasers, the continuous subbands are generally neglected. However, it has been demonstrated in the studies of 630 nm band GaInP/AlGaInP lasers[15,17] and our previous work[14] that the optical transitions involving spillover electrons play an important part in the threshold current. In this study the main interest is focused on the spillover effect on the laser threshold. So, we ignore the electron leakage to the p-type cladding and any indirect interband transitions.

The valence band structure is calculated based on the six-band $\mathbf{k}\cdot\mathbf{p}$ model which includes the coupling of the heavy-hole, the light-hole, and the spin-orbit split-off bands.[18,19] The strain effect is also included. The formulas for calculating the valence bands can be found in our previous work.[14] For conduction band states, we use the single-band effective-mass equation,

$$\left[-\frac{d}{dz}\frac{\hbar^2}{2m_z(z)}\frac{d}{dz}+V_{\text{eff}}(z)\right]\varphi=E\varphi, \tag{1}$$

$$V_{\text{eff}}(z)=\frac{\hbar^2k_t^2}{2m_t(z)}+E_c^0(z)+P_{c\epsilon}(z), \tag{2}$$

to solve the envelope functions φ and the energy E, where m_z (m_t) is the electron effective mass in the direction along (transverse to) the growth direction, $E_c^0(z)$ is the z-dependent conduction band edge of the undeformed materials composing the heterostructure, and $P_{c\epsilon}$ is the hydrostatic energy shift in the conduction band. Once the energy states of both the valence and the conduction subbands have been solved, the momentum matrix elements can be obtained using the formulas in Refs. 14 and 20.

The dopants are assumed to be introduced into the barriers around the QW. For convenience, we also assume that the carriers released from the dopants are all relaxed to the well region. The charge neutrality in the active region then allows us to write

$$p_s+N_{D,s}^+=n_s+N_{A,s}^-, \tag{3}$$

where p_s, n_s, $N_{D,s}^+$, and $N_{A,s}^-$ are the sheet concentrations of holes, electrons, ionized donors, and ionized acceptors, respectively. Here we use the sheet concentrations instead of the volume concentrations to avoid the complexity arising from the penetration of the bound wave functions into the barriers. For a given ionized acceptor (or donor) concentration, one can obtain the quasi-Fermi levels of the conduction bands F_c and the valence bands F_v as functions of the carrier concentrations. Consequently, the Fermi-Dirac distributions of carriers in energy can be determined. One can then further obtain the gain spectrum, the spontaneous emission spectrum, and the current density due to radiative recombinations. The related formulas can be found from our previous work.[14]

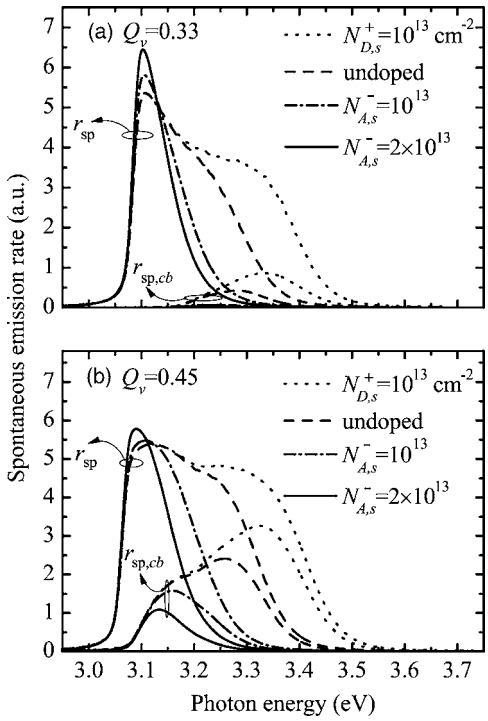

FIG. 2. The spectra of the total spontaneous emission rate r_{sp} and one of its components, $r_{sp,cb}$, at threshold for 3.6 nm $In_{0.2}Ga_{0.8}N/GaN$ single-QW LDs with various doping levels for Q_v=0.33 in panel (a) and Q_v=0.45 in panel (b). The $N_{D,s}^+$ and $N_{A,s}^-$ are the sheet concentrations of ionized donors and acceptors, respectively.

III. RESULTS AND DISCUSSION

In this section we present and discuss the calculated results of the spontaneous emission spectra and the current densities for modulation-doped $In_{0.2}Ga_{0.8}N/GaN$ QW lasers at threshold. The EBL is an $Al_{0.2}Ga_{0.8}N$ layer. The widths of the QW and the EBL are fixed at 3.6 and 20 nm, respectively, for all structures. For the double-QW structure, a 6 nm GaN barrier is inserted between the wells. All the values of material parameters used in our calculation can be found from Ref. 21 for wurtzite GaN, InN, and AlN. For the ternary compounds InGaN and AlGaN, the parameters are obtained by the linear interpolation between the binary compounds, except those already given in Ref. 21. The depth of the well is an important factor that influences the spillover of carriers, but until now there have been no unambiguous values for the band offset of the nitride heterointerfaces. We thus take the valence band partition ratio Q_v as a variable parameter, where $\Delta E_v = Q_v \Delta E_g$ (ΔE_v and ΔE_g being the valence band offset and the band gap difference, respectively). The confinement factor for the lasers is assumed to be $3 \times 10^{-3} L_a$, where L_a is the active region width in units of nanometers. The total loss of the cavity α and the temperature T are set at 60 cm^{-1} and 300 K, respectively, except in the case where they are considered as variable parameters.

Figure 2 shows the spectra of the total spontaneous emission rate r_{sp} and one of its components, $r_{sp,cb}$, at threshold for single-QW structures with various doping levels, assuming Q_v=0.33 in panel (a) and Q_v=0.45 in panel (b). Because the valence subbands have very high densities of states, all the holes almost lie at the bottom of the well. This leads to a negligibly small amount of holes spilling over from the well. Hence, it is found from our calculated results that the bc and cc transitions are negligible compared with the bb and cb transitions. This permits us to write $r_{sp} \simeq r_{sp,bb} + r_{sp,cb}$. Therefore, henceforth we will not present the calculated results concerning transitions involving the continuous valence subbands. As shown in Fig. 2, the shapes of r_{sp} are broadened because of the appearance of $r_{sp,cb}$. This phase space filling effect was observed in a recent experimental work.[22] The shapes of r_{sp} are broader for Q_v=0.45 than those for Q_v=0.33 due to the larger contribution of $r_{sp,cb}$ for Q_v=0.45. For a shallower electron QW, the bound subband is closer to the continuous subbands. Therefore, there are more electrons spilling to the continuous subbands, resulting in the larger $r_{sp,cb}$.

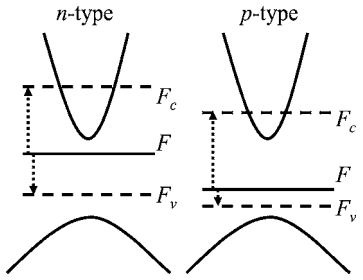

FIG. 3. Schematic diagrams of the conduction and the valence bands together with the Fermi level F, and the quasi-Fermi levels F_c and F_v at threshold for the cases of n-type doping (the left) and p-type doping (the right).

It is noticed that the LDs with p-type doping have smaller $r_{sp,cb}$ at threshold than the undoped one, while the one with n-type doping has a larger $r_{sp,cb}$. This gives rise to the narrowing of r_{sp} for p-type doping and the broadening of r_{sp} for n-type doping, as shown in Figs. 2(a) and 2(b). As expected, the p-type doping alleviates the electron spillover while the n-type doping worsens it. To further understand the dependence of electron spillover on the doping level and species, we appeal to the diagram in Fig. 3, where there are schematically the conduction and valence bands together with the Fermi level F, and the quasi-Fermi levels F_c and F_v at threshold. The levels F, F_c, and F_v lie at upper positions for n-type doping than for the undoped, while for p-type doping the levels lie at lower positions, as illustrated in Fig. 3. Furthermore, because of the large asymmetry in density of states between the conduction and valence bands, the quasi-Fermi level F_c is much more sensitive to the doping level than F_v. For n-type doping, the high position of F_c implies serious electron spillover at threshold which causes the broadening of r_{sp}, as has been shown in Fig. 2. On the contrary, the p-type doping has a lower F_c and hence can diminish the electron spillover. This can also reduce the thermionic emission current leaking across the EBL. Besides, it is difficult for the p-type doping to cause the hole spillover because of the large density of states of the valence bands. As the spillover becomes negligibly small, further increasing the p-type doping level will not be a benefit, but causes an increase in the spontaneous emission rate at threshold. This is reflected by the increase of r_{sp} at energy about the main peak with the p-type doping level, as shown in Fig. 2.

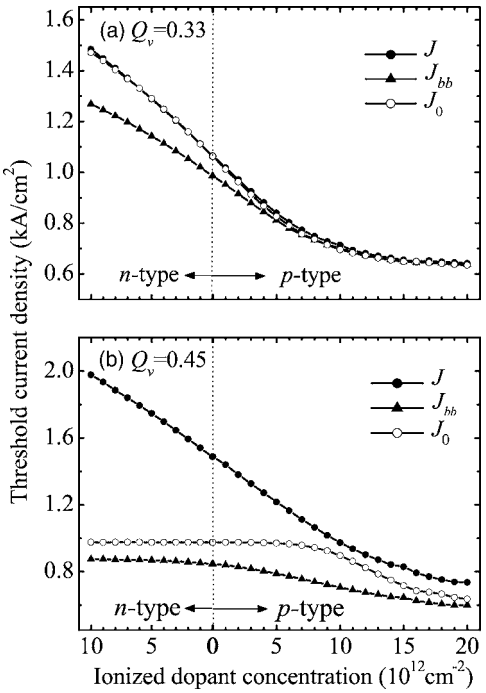

FIG. 4. The current densities, J, J_{bb}, and J_0, at threshold vs the ionized dopant concentration for 3.6 nm $In_{0.2}Ga_{0.8}N/GaN$ single-QW LDs, assuming Q_v=0.33 in panel (a) and Q_v=0.45 in panel (b). The J is the total threshold current density, the J_{bb} is the current density due to the bound-to-bound process, and the J_0 is the threshold current density calculated without considering the carrier spillover.

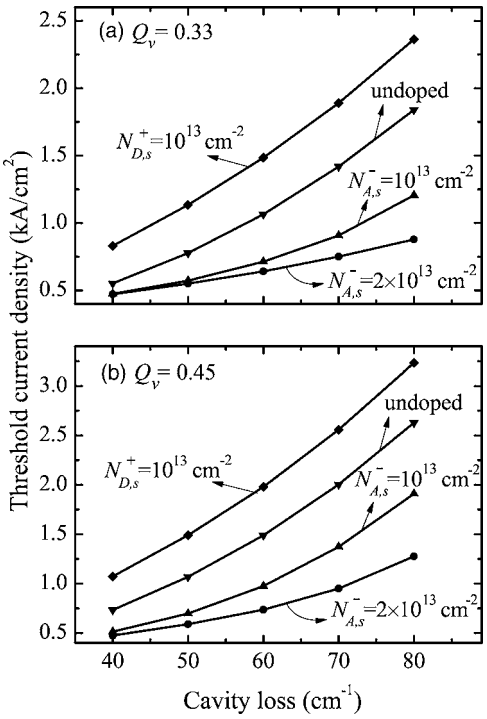

FIG. 5. The current densities, J, at threshold as functions of the cavity loss for 3.6 nm $In_{0.2}Ga_{0.8}N/GaN$ single-QW LDs with various doping levels for Q_v=0.33 in panel (a) and Q_v=0.45 in panel (b).

Figure 4 shows the current densities J, J_{bb}, and J_0 at threshold versus the ionized dopant concentration for single-QW structures, similarly assuming the partition ratio Q_v=0.33 in panel (a) and Q_v=0.45 in panel (b). Here, for comparison, we include the current density J_0 which is calculated with all the carriers occupying the bound subbands. The difference $J-J_{bb}\simeq J_{cb}$ can reveal the influence of electron spillover on the total current density J at threshold. As expected, both J_{bb} and J_{cb} decrease with the p-type doping level but increase with the n-type doping level. As the p-type doping level is very high (about 1.5×10^{13} cm^{-2} for Q_v =0.33 and about 2×10^{13} cm^{-2} for Q_v=0.45), the benefit from the p-type doping vanishes and the current density J seems to approach an asymptotic value. In practice, such high p-type doping is difficult to achieve in the nitride compounds due to the large activation energy of acceptors.

It is noticed that the current density J_0 behaves quite differently from J for Q_v=0.45, implying that it is important to consider the electron spillover in calculation of the threshold current for a shallow QW. Peculiarly, the J_0 is almost fixed at a constant value (~1 kA/cm^2) in the whole range of n-type doping level and also for p-type doping level less than $\sim7\times10^{12}$ cm^{-2}. This can be explained from Eq. (2), where we find $m_t(z)$ a function of z. It has a smaller value inside the QW region than outside. With k_t increasing, the effective potential energy V_{eff} increases more inside the QW region than outside. For k_t beyond a certain critical value k_c, the V_{eff} forms a barrier profile with a higher effective potential energy inside the QW region than outside. In this case, the wave function is leaky in nature and has a nearly zero overlap with the wave function of the valence band state. Thus, the electrons at states of $k_t>k_c$ have nothing to do with the interband process. This explains the peculiar behavior of J_0. This behavior is particularly obvious for a shallow QW (for instance, Q_v=0.45) because of the small value of k_c. In the practical case, the threshold current density J varies with the n-type doping level because of the electron spillover to the continuous subbands.

Until now the calculated results have been for LDs with a cavity loss of 60 cm^{-1}. For a higher cavity loss, it requires a higher carrier density in the QW to reach threshold. In this case, the problem of electron spillover becomes more important. Figure 5 shows the threshold current density J as a function of the cavity loss α of single-QW LDs with different doping levels for (a) Q_v=0.33 and (b) Q_v=0.45. As expected, the J increases with α. The increase is particularly obvious for the case of n-type doping (as well as for the case of the undoped). Moreover, most of the curves are somewhat superlinear because the spillover electrons play a more and more important role with α increasing in the interband process. As we have learned, the p-type doping can significantly diminish the electron spillover. This is further evidenced by the fact in Fig. 5 that the separation between the curve for the undoped and the one for $N_{A,s}^-=2\times10^{13}$ cm^{-2} increases with the cavity loss α. By p-type doping, the threshold current density for α=80 cm^{-1} can be reduced by a factor of ~2 for Q_v=0.33 (J=1.8 kA/cm^2 for the undoped and J =0.8 kA/cm^2 for $N_{A,s}^-=2\times10^{13}$ cm^{-2}) and by a factor of ~1.5 for Q_v=0.45 (J=2.7 kA/cm^2 for the undoped and J =1.8 kA/cm^2 for $N_{A,s}^-=2\times10^{13}$ cm^{-2}). For the large cavity loss, the reduction in J is more considerable for Q_v=0.33 than for Q_v=0.45 because the electron spillover can almost be eliminated for the deep well by the p-type doping but is

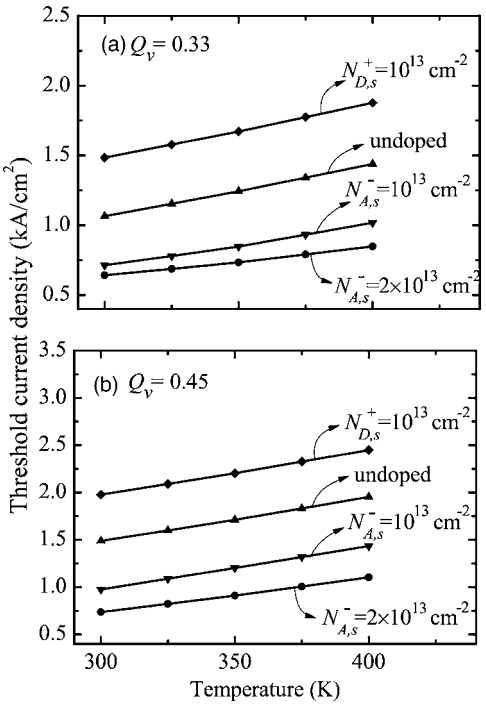

FIG. 6. The current densities, J, at threshold vs temperature for 3.6 nm $In_{0.2}Ga_{0.8}N/GaN$ single-QW LDs with various doping levels for Q_v=0.33 in panel (a) and Q_v=0.45 in panel (b).

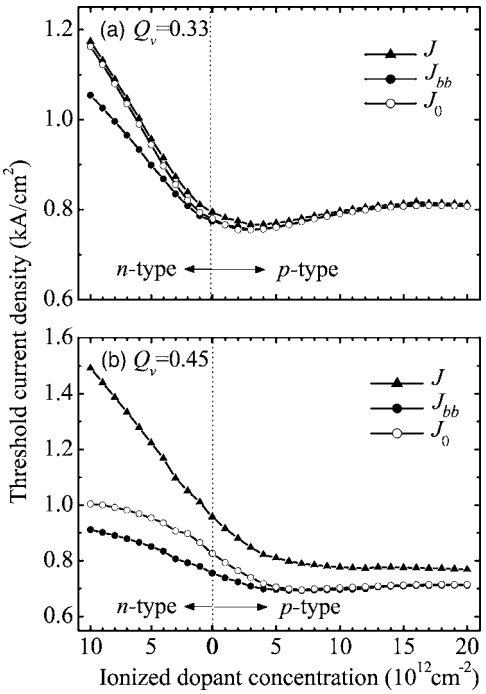

FIG. 7. The current densities, J, J_{bb}, and J_0, at threshold vs the ionized dopant concentration for 3.6 nm $In_{0.2}Ga_{0.8}N$–60 nm GaN double-QW LDs, assuming Q_v=0.33 in panel (a) and Q_v=0.45 in panel (b).

not negligible for the shallow well. This reflects the fact that with the p-type doping $N_{A,s}^{-}=2\times10^{13}$ cm^{-2}, the J-α curve is almost linear for Q_v=0.33 but obviously nonlinear for Q_v =0.45.

The temperature characteristic is also an important issue for lasers. We plot the threshold current density J versus temperature T with various doping levels for single-QW LDs in Fig. 6, assuming Q_v=0.33 in panel (a) and Q_v=0.45 in panel (b). It can be seen that the J-T curves are linear and almost parallel to each other. It seems that introducing dopants to the active region does not significantly influence the temperature characteristic. However, the situation will not be the case if the electron leakage into the p-type cladding layer is considered. As has been pointed out, such leakage is serious for n-type doping[17] and further deteriorates at high temperature. The p-type doping can used to reduce the electron leakage into the p-type cladding layer as well as the electron spillover.

In Fig. 7, the current densities J, J_{bb}, and J_0 at threshold of double-QW LDs are plotted as functions of the ionized dopant concentration for (a) Q_v=0.33 and (b) Q_v=0.45. Similar to the case in Fig. 4, the $J_{cb}(\simeq J-J_{bb})$ and the amount of spillover electrons increase with the n-type doping level while decrease with the increase of p-type doping level. Compared with the case of single-QW LDs, the electron spillover is smaller for the double-QW LDs because of the smaller carrier density required for threshold. As a result, the J_{bb} has a minimum at a certain p-type doping level and increases as the p-type doping level further increases. In this situation, the drawback of increasing electron-hole recombination goes beyond the advantage of reducing electron spillover. The J_{bb} reaches the minimum at about 2.5 $\times10^{12}$ cm^{-2} for Q_v=0.33 and at about 5$\times10^{12}$ cm^{-2} for Q_v=0.45, where the threshold current density J reaches or approaches the minimum value.

Comparing the threshold current densities in Fig. 4 and those in Fig. 7, one can see that the favorite structure for the lowest J is the single-QW one with heavily p-type doping for both Q_v=0.33 and Q_v=0.45. However, in reality, the high activation energy of acceptors in the wide-gap nitride compounds may make such optimization difficult to achieve. If the heavily p-type doping could not be achieved, the double-QW structure with a lower p-type dopant concentration is a good choice. The optimized p-type doping levels are about 2.5$\times10^{12}$ cm^{-2} ($\sim$6.9$\times10^{18}$ cm^{-3}) for Q_v=0.33 and about 7$\times10^{12}$ cm^{-2} ($\sim$1.9$\times10^{19}$ cm^{-3}) for Q_v=0.45. The ionization efficiency depends on the doping level and is still unclear for p-type modulation-doped InGaN/GaN QWs. From the experimental work with structures similar to those used here, a uniformly doped 4 nm $In_{0.2}Ga_{0.8}N$/4 nm GaN supperlattice with a Mg concentration of 3$\times10^{19}$ cm^{-3} has a spatially averaged hole concentration of about 2.6 $\times10^{19}$ cm^{-3}.[23] Since the main contribution of released holes is from the acceptors in the GaN barriers, the ionization efficiency of the modulation doping is about 100%. Thus, the optimized carrier concentrations mentioned above are possible to be achieved.

IV. CONCLUSION

The radiative current densities and the spontaneous emission spectra in modulation-doped InGaN/GaN QW LDs have been investigated with the electron spillover above the barriers considered. The calculated results indicate that the consideration of electron spillover is important in studying

the effects of modulation doping to the active region especially for shallow electron QW structures. When the influence of introducing impurities on crystal quality is ignored, the threshold current density can be significantly reduced by *p*-type doping, but increased by *n*-type doping which is conventionally used. The benefit from the *p*-type doping is particularly obvious for a large cavity loss. An optimized low threshold current can be achieved for single-QW LDs with heavily *p*-type doping. For double-QW LDs, more slightly *p*-type doping is required to obtain low threshold current.

ACKNOWLEDGMENTS

This work was supported by the National Science Council under Grant No. 95-2221-E-009-281 and MOE ATU Program of Republic of China.

[1]S. Nakamura, T. Mukai, and M. Senoh, J. Appl. Phys. **76**, 8189 (1994).
[2]D. E. Eason, Z. Yu, W. C. Hughes, W. H. Roland, C. Boney, J. W. Cook, Jr., J. F. Schetzina, G. Cantwell, and W. C. Harasch, Appl. Phys. Lett. **66**, 115 (1995).
[3]S. Nakamura, M. Senoh, S. Nagahama, N. Iwasa, T. Yamada, T. Matsushita, H. Kiyoku, and Y. Sugimoto, Jpn. J. Appl. Phys., Part 2 **35**, L74 (1996).
[4]J.-Y. Chang and Y.-K. Kuo, J. Appl. Phys. **93**, 4992 (2003).
[5]M. Hansen, J. Piprek, P. M. Pattison, J. S. Speck, S. Nakamura, and S. P. Denbaars, Appl. Phys. Lett. **81**, 4275 (2002).
[6]S.-N. Lee, S. Y. Cho, H. Y. Ryu, J. K. Son, H. S. Paek, T. Sakong, T. Jang, K. K. Choi, K. H. Ha, M. H. Yang, O. H. Nam, Y. Park, and E. Yoon, Appl. Phys. Lett. **88**, 111101 (2006).
[7]S. P. Lepkowski and S. Krukowski, J. Appl. Phys. **100**, 016103 (2006).
[8]S. Nakamura, M. Senoh, S. Nagahama, N. Iwasa, T. Yamada, T. Matsushita, Y. Sugimoto, and H. Kiyoku, Appl. Phys. Lett. **70**, 1417 (1997).
[9]S. Bidnyk, T. J. Schmidt, Y. H. Cho, G. H. Gainer, J. J. Song, S. Keller, U. K. Mishra, and S. P. DenBaars, Appl. Phys. Lett. **72**, 1623 (1998).
[10]Y.-H. Cho, J. J. Song, S. Keller, M. S. Minsky, E. Hu, U. K. Mishra, and S. P. DenBaars, Appl. Phys. Lett. **73**, 1128 (1998).
[11]S. Keller, S. F. Chichibu, M. S. Minsky, E. Hu, U. K. Mishra, and S. P. DenBaars, J. Cryst. Growth **195**, 258 (1998).
[12]F. Della Sala, A. Di Carlo, P. Luigi, F. Bernardini, V. Fiorentini, R. Scholz, and J. Jancu, Appl. Phys. Lett. **74**, 2002 (1999).
[13]G. Franssen, T. Suski, P. Perlin, R. Bohdan, A. Bercha, W. Trzeciakowski, I. Makarowa, P. Prystawko, M. Leszczynski, I. Grzegory, S. Porowski, and S. Kokenyesi, Appl. Phys. Lett. **87**, 041109 (2005).
[14]S. J. Huang and S. T. Yen, J. Appl. Phys. (to be published).
[15]S. T. Yen and C. P. Lee, IEEE J. Quantum Electron. **33**, 443 (1997).
[16]S. T. Yen, Phys. Rev. B **66**, 075340 (2002).
[17]S. T. Yen and C. P. Lee, IEEE J. Quantum Electron. **34**, 1644 (1998).
[18]S. L. Chuang and C. S. Chang, Phys. Rev. B **54**, 2491 (1996).
[19]F. Mireles and S. E. Ulloa, Phys. Rev. B **60**, 13659 (1999).
[20]S. L. Chung, IEEE J. Quantum Electron. **32**, 1791 (1996).
[21]I. Vurgaftman and J. R. Meyer, J. Appl. Phys. **94**, 3675 (2003).
[22]Y. J. Wang, S. J. Xu, Q. Li, D. G. Zhao, and H. Yang, Appl. Phys. Lett. **88**, 041903 (2006).
[23]K. Kumakura, T. Makimoto, and N. Kobayashi, Jpn. J. Appl. Phys., Part 2 **39**, L195 (2000).